University of Zawia Journal of Engineering Sciences and Technology (UZJEST)
Volume 3, Issue 2, (2025), pp 288-307, ISSN 3006-2764

Design of a PV Solar-Covered Parking System for the College of Renewable Energy Tajoura, Libya: A PVsyst-Based Performance Analysis

Ibrahim Imbayah*[1], Ahmed belghasem[1], Alfarouk AlAshhab[1], Mohammed Maqra[1], Yasser F. Nassar[2], Mohamed Khaleel[3]

[1]Department of Energy Engineering, College of Renewable Energy, Tajoura, Libya

[2]Mechanical and Renewable Energy Eng. Dept., Faculty of Eng., Wadi Alshatti University, Libya

[3]Department of Electrical-Electronics Eng., Faculty of Engineering, Karabuk University, Karabuk, Turkey

*Corresponding author email: ibrahim.alzayani@gmail.com

Received: 19-11-2025 | Accepted: 14-12-2025 | Available online: 15-12-2025 | DOI:10.26629/uzjest.2025.23

ABSTRACT

The paper presents the design and performance simulation of a 78 kW grid-connected solar PV system installed in the parking canopy of the College of Renewable Energy and the Tajoura Kidney Hospital in Libya, designed to meet the college and hospital's distinct loads through three inverters (1 × 20 kW, 2 × 50 kW) with 150 monocrystalline 525W modules oriented due south with a tilted elevation of 30°. The PVsyst software simulates performance, producing 128,964 kWh per year of solar AC energy, with related parameters of 83.37% performance ratio and 1,637 kWh/kWp/year solar yield. Loss components show the major contribution of soiling (2.0%), temperature (2.04%), conversion (2.38%), and unavailability (0.41%). Economic parameters give an LCOE between $0.052 & $0.057 per kWh with a simple payback of 6-7 years. The solar PV meets approximately 49% of the combined institutional demand, along with the export of approximately 123,757 units per year. Probabilistic yield estimation gives the 90th percentile yield of 123.28 MWh/year. The annual avoidance of CO_2 is 70.93 metric tons. The approach presented in this paper presents a practical way to implement solar carports in institutional settings in the North African region.

Keywords: Photovoltaic systems (PV), PVsyst, Solar carport, Monocrystalline, Grid-Connected, Libya.

تصميم نظام مواقف سيارات مغطى بألواح شمسية كهروضوئية لكلية الطاقة المتجددة في تاجوراء – ليبيا: تحليل الأداء باستخدام برنامج (PVsyst)

إبراهيم إمبيه*[1]، أحمد بلقاسم[1]، فاروق الأشهب[1]، محمد مقرا[1]، ياسر نصار[2]، محمد خليل[3]

[1]قسم هندسة الطاقة، كلية الطاقة المتجددة، تاجوراء، ليبيا

[2]قسم الهندسة الميكانيكية والطاقة المتجددة، كلية الهندسة، جامعة وادي الشاطئ، ليبيا

[3]قسم الهندسة الكهربائية والإلكترونية، كلية الهندسة، جامعة كارابوك، كارابوك، تركيا

ملخـــــص البحـــــث

تقدم هذه الورقة تصميم ومحاكاة أداء نظام طاقة شمسية كهروضوئية بقدرة 78 كيلوواط متصل بالشبكة ومركب في موقف السيارات المغطى بكلية الطاقة المتجددة ومستشفى تاجوراء للكلى في ليبيا، وهو مصمم لتلبية الأحمال المختلفة للكلية والمستشفى من خلال ثلاثة محولات (1 × 20 كيلوواط، 2 × 50 كيلوواط) مع 150 وحدة أحادية بلورية 525 واط موجهة نحو الجنوب بزاوية ميل 30 درجة. يقوم برنامج **PVsyst** بمحاكاة الأداء، حيث ينتج 128,964 كيلوواط ساعة سنويًا من الطاقة الشمسية المترددة، مع معلمات ذات صلة بنسبة أداء 83.37٪ وعائد شمسي 1,637 كيلوواط ساعة/كيلوواط/سنة. تُظهر مكونات الخسارة المساهمة الرئيسية للتلوث (2.0٪) والحرارة (2.04٪) والتحويل (2.38٪) وعدم التوافر (0.41٪). تعطي المعلمات الاقتصادية تكلفة **LCOE** بين 0.052 و0.057 دولار لكل كيلوواط ساعة مع فترة استرداد بسيطة تتراوح بين 6 و 7 سنوات. تفي الطاقة الشمسية الكهروضوئية بحوالي 49٪ من الطلب المؤسسي الإجمالي، إلى جانب تصدير حوالي 123,757 وحدة سنويًا. يعطي تقدير العائد الاحتمالي عائدًا بنسبة 90٪ يبلغ 123.28 ميجاوات ساعة/سنة. يبلغ تجنب انبعاثات ثاني أكسيد الكربون السنوية 70.93 طنًا متريًا. يقدم النهج المطروح في هذه الورقة طريقة عملية لتنفيذ مواقف السيارات الشمسية في المؤسسات في منطقة شمال إفريقيا.

الكلمات الدالة: الأنظمة الكهروضوئية (PV)، برنامج PVsyst، موقف سيارات شمسي، أحادي البلورة، متصل بالشبكة، ليبيا.

1. Introduction

Driven by concerns about climate change and global warming, the global installed capacity of renewable energy grew by 50% in 2024. In the end of 2024, the global installed capacities of renewables such as solar, wind, hydropower, geothermal, marine, biogas, etc reached about 4,448.1 GW, from them 1,600 GW for PV solar energy systems, 1,021 GW for wind energy, about 96.8 GW electricity from biomass energy, the geothermal energy reached 16,873 MWe, and hydropower capacity stood at nearly 1,450 GW at the end of 2024. This growth in the RE market reflects a global shift towards renewable and sustainable energy technologies [1,2]

Libya is also concerned with these international efforts to reduce pollution and mitigate environmental damage, as one of the countries that has ratified the Paris Agreement on climate change. It also has a declared strategy towards transitioning to clean and renewable energy, which states that the share of renewable energy in the energy mix should exceed 50% by 2050 [3]. In this context,

Libya, a country with highly adequate solar power and large electricity demand, derives more than 95% of its electric power from hydrocarbon sources, incurring costs in terms of fuel subsidy bottlenecks and greenhouse gas emissions [3]. Institutional buildings such as universities, hospitals, and governmental buildings have been identified as highly attractive projects for implementing solar PV technology based on their concurrent daytime electricity load demands and large parking areas. Solarized parking garages have been recognized as a new innovative technology that serves a double purpose of electricity power harvesting while simultaneously offering protection to cars, fully exploiting infrastructure without occupying new land areas [4].

This particular setup fulfills several aims at once, including electricity harvesting, shading, mitigation of urban heat islands, and providing a successful demonstration of a renewable technology implementation. College of Renewable Energy in Tajoura, Libya, located at geographical coordinates 32.815 N and 13.533E, and its neighbor, Tajoura Kidney Hospital, also face common issues related to electricity infrastructure. Overall maximum electricity demand is 78 kW, while its renal dialysis unit demands a constant electricity power supply. Building rooftops are not suitable for a solar power

installation turnaround because of irregular orientations, as well as their inaccessibility issues in terms of building rooftop maintenance. On a similar note, a 1,600 m² parking lot lacks suitable shading, causing substantial vehicle interior heating above 40°C when surrounding temperatures soar above 40°C in summer conditions. Land-engrossing ground-mounted arrangements will hamper land use, while rooftop arrangements will again face the aforementioned issues [5].

Consequently, a question that arises in research is as follows: How will a Tajoura's particular climate and operational setup of a solar parking lot infrastructure be most appropriately designed in order to powerfully exploit its electricity harvesting formulation capabilities with a supreme objective to become a multi-functional setup? Recent studies have also outlined several examples of implemented solar parking lot projects around different geographical areas of our globe and have quantitatively analyzed economic feasibility of electricity harvesting capabilities of a parking lot infrastructure in hospitals at present in the USA, and have quantitatively supported performance ratios of 78%-82% productivity at 1,420–1,580 kW of annual electricity harvesting in temperate climate conditions [6].

Explored the optimal tilt angles of urban PV carport systems, proving an improvement in power output of 2-5% by tilt angle optimization [7]. Modeled a PV carport system for Cairo University by using PVsyst software, resulting in a PR of 81.3% at a specific yield of 1,589 kWh/kWp/year [8]. Regional research has been done to explore North African countries' solar power capabilities. The International Renewable Energy Agency (IRENA) analyzed renewable energy opportunities within the region and found solar PV to be the most economically attractive technology for swift implementation [9].

Nevertheless, a substantial gap is present in existing research pertaining to methods of optimization in North African coast conditions, approaches to integrated healthcare and education facilities, as well as overall system performance analysis using a sophisticated simulation package validated through localized meteorological conditions. This research work presents several additions to existing knowledge in the field of solar energy engineering in terms of:

1. Comprehensive Design Toolset and Methodology: Combining various specialized software packages (for instance, SketchUp 3D modeling of structures, Global Solar Atlas, and NASA POWER climate data, and PVsyst simulation software) that deliver higher modeling ability than those of individual software packages.
2. Site-Specific Performance Data: Simulation of system performance in the Libyan Mediterranean environment, addressing a void in current solar installation technical publications within that region.
3. Dual Institutional Load Analysis: Evaluation of electrical architecture planning related to supporting critical (hospital) loads and non-critical (educational) loads from a common generating resource.
4. Economic Validation: In-depth economic analysis work that incorporates Levelized Cost of Energy (LCOE) analysis, Net Present Value (NPV) criteria, and probabilistic forecasting of a power plant's output as pertains
5. Replicable Framework: Development of a set of design principles that could be applied to similar institutional projects within Libya and its surrounding countries.

This paper is divided into its remaining portions. In Section II, a detailed methodology is described. In Section III, detailed results have been introduced. In Section IV, a discussion related to performance analysis, optimization, comparison of current work with previous ones in the form of analysis from different studies, and its implications, is carried out. Finally, in Section V, concluding remarks have been drawn.

2. Methodology of the study site

2.1 Study Site Characterization

Our case study site is Al-Bayda city, Libya, that located in the northeast part of the country, in the Jabal Al-Akhdar in the Cyrenaica area. Two PV modules of the same type were mounted next to each other on a non-tracking mounting system with the same tilt and azimuth angle in order to have the same solar irradiance on the two modules. The site of the experiment was the rooftop of a residential building in Al-Bayda (32.7627°N, 21.7551°E), which is 632 meters above sea level. The residential building is located adjacent to a high density of traffic and an industrial area that encompasses construction material sales such as gravel, sand, and cement, marble manufacturing, and automotive repair workshops, as well as numerous local factories. In the following figure 1 shown Key climatic parameters for Tajoura city: (a) Global solar irradiation, Wh/m^2, (b) Ambient Temperature, °C, and (c) Wind speed, m/s at 10 above the ground.

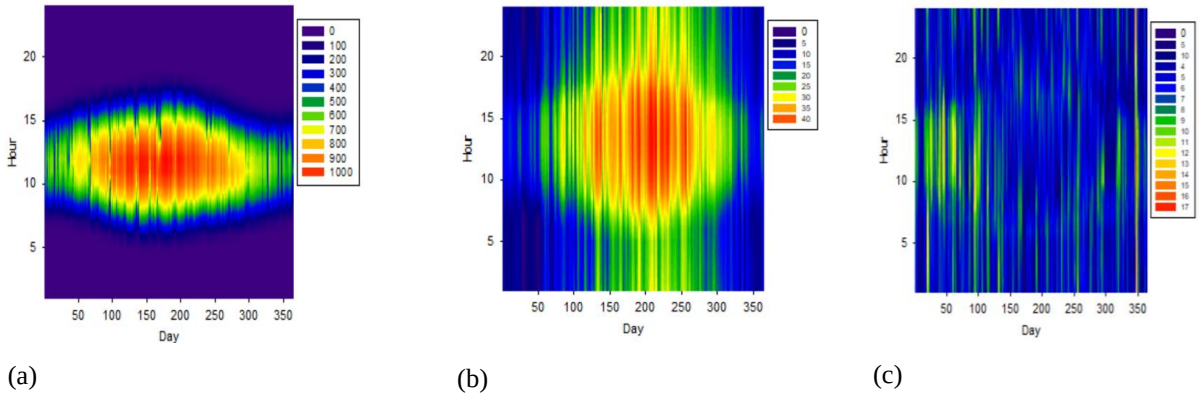

Figure 1. Key climatic parameters for Tajoura city: (a) Global solar irradiation, Wh/m2, (b) Ambient Temperature, °C, and (c) Wind speed, m/s at 10 above the ground [10].

2.2 Load Assessment and Energy Demand Analysis

Electrical load characterization was done through digital voltmeter measurements of power consumption in real-time. It is noted that the College of Renewable Energy, consisting of administrative offices, lecture halls, labs, a theater, and ancillary facilities, has a peak load demand of 20 kW during daylight hours of operation. Similarly, Tajoura Kidney Hospital's dialysis unit and medical equipment have a total power consumption of 58 kW in a continuous process. Overall, a total peak load of 78 kW is recorded at mid-day hours, when peak solar output is also possible, and thus will have a positive effect on self-consumption rates. There is an analysis of load data in terms of consumption in different hours of the day. Colleges have a usual pattern of load consumption, peaking between 8:00 and 17:00 hours. This is similar to hospitals that run for 24 hours, peaking in daylight hours of higher usage in dialysis.

2.3 Component Selection

1) Photovoltaic Modules

According to the results obtained by local researchers [11-13], Aleo solar S59Y310 Monocrystalline silicon modules (rated power of 525 W) have been chosen after considering a number of criteria. The technology used in these modules is Half-cut cell technology, which enables better performance in case of shading conditions and also minimizes resistive losses [14]. The major specifications of the module are as follows: efficiency of 20.36%, power-temp. coefficient of -0.34 %/°C for max. power, and its size measures 2.278 m x 1.134 m. This large module size of 2.6 m² allows more shading coverage with fewer

modules, thereby making it simpler to install with fewer points of failure. In total, 150 modules have been considered in three parallel arrays of 50 modules in each, giving a total capacity of 78.75 kW. Also, the number of modules has been optimized depending upon the load requirement, parking space availability, and economic feasibility.

2) Inverters

Grid-connected inverters supplied by Perfect Galaxy: EQX0500UV 320XP(N) 320V were chosen based on their high rate of efficiency and ability to withstand similar climatic conditions, and the recommendation of local researchers [15]. The power system consists of three inverters, one 20 kW inverter for the college load, and two 50 kW inverter units for the hospital load. This setup benefits in several ways:

• Independent Subsystems: Independent operation is possible through separate institutional loads.

• Redundancy: is offered at an N+1 level by the two hospital-grade

• Optimal Loading: Hospital UPS systems run at an average of 58% of their capacity or 29 kW per inverter.

• MPPT Optimization: MPPT inputs for multiple strings (2 per 20 kW of unit capacity, 4 per 50 kW of unit capacity) support string-level MPPT optimization.

Inverter capacity of 120 kW stands at an oversizing ratio of 1.52 pertaining to its array capacity, which is suitable for maximizing overall annual power production as well as allowing for degradation of individual modules within a lifetime of the system [16].

2.4 Electrical System Architecture

In its electrical configuration, it uses a series string connection to keep resistive losses low. The college system connects 38 modules in two strings of 19 modules per string, linking to two MPPT inputs of the 20 kW inverter. String voltage is designed to keep a DC range of 600 to 1,000 volts across all temperatures. Electrical single-line diagram of the overall system architecture. This is an array configuration of 150 units in three parallel strings, depicting Series String Electricity Configuration (2 x 19 strings in college system, 8 x 14 strings in college system) with Inverter MPPT inputs divided over three units, DC Combiners, AC distribution panels, as well as a grid connection point with a metering point.

Hospital Subsystem: In this subsystem, 112 modules are interconnected through eight strings of 14 modules in two 50 kW inverters. This is done in order to balance well the current load of MPPT inputs while at the same time ensuring that it is within inverter specifications. In effect, DC cables are provided with adequate protection through routing that is underground. This is as seen in Figure 2.

Figure 2. layout of the PV/Grid system

2.5 Structural Design

To verify its strength, a 3D model of a support structure was created using “SketchUp.” This support structure design includes:

- Foundations: Bases of reinforced concrete (1.90 m x 1.60 m x 0.40 m - burial depth) supporting main columns, complete with observable pedestals of 0.60 m x 0.60 m x 0.40 m for vehicle impact protection.
- Main Columns: Wide-flange steel columns of height 3.35m, hot-dip galvanized to offer protection against corrosion, at an interval of 5 m.
- Horizontal Beams: Wide-flange steel of 6.15 m length, sloped at an angle of 30°.
- Mounting Rails for Modules: Aluminum extrusions of 5 m length fixed at 1.30 m intervals to horizontal beams, supporting five modules per rail.

3D Structural Model of Solar Carport System developed in SketchUp. This 3D image of a solar carport system highlights the following components of the system: (a) Bury concrete foundation with protective pedestals, (b) Main column of 3.35 m height hot-dip galvanized, (c) Horizontal supporting beams at an inclination of 30°, (d) Aluminum module supporting rails at an interval of 1.30 m, and (e) 150 solar panels of 50 modules in three rows. In this 3D image, the inter-column spacing of 5 m is visible, column extensions for expansion capabilities of 0.10 m, and a clearance of 7 m at a minimum height ensures sufficient shade for vehicles. Color coding of columns is orange, horizontal supporting beams in green, and supporting rails in blue. The structure is designed to resist 50-year return period wind load conditions (design wind speed of 45 m/s) and moderate seismic activities (0.10 - 0.15 g) characteristic of Libya's coast. Material selection focuses on longevity in a maritime environment by considering galvanized steel and aluminum materials. An expansion plan is also incorporated in the design by means of 0.10 m column extensions that will accommodate extra rows of modules.

2.6 System Orientation and Tilt Angle Optimization

System orientation was optimized through analysis of solar geometry and site constraints. The array faces true south (180° azimuth) to maximize solar exposure throughout the year. Sensitivity analysis in the Global Solar Atlas confirmed this orientation captures 100% of optimal annual irradiation, with deviations of ±10° reducing production by less than 1% [17].

Tilt angle selection balanced competing objectives: summer optimization (20-25° ideal), winter optimization (35-40° ideal), self-cleaning capability (>25° enables dust shedding), and structural efficiency. A fixed 30° tilt was selected based on PVsyst parametric studies showing this angle achieves 98.2% of the theoretical maximum with seasonally-adjusted tracking while providing superior self-cleaning compared to lower angles.

Parametric analysis of yearly power output as a function of tilt angle, based on simulation by PVsyst. This clearly shows that our chosen tilt of 30° (red circle) will produce 128,964 kWh per year, getting 98.2% of the theoretical maximum possible annual power output of 131,318 kWh, taking into account 22° to 38° tilt positions according to seasons. Other tilt positions of 25° and 35° will produce 127,842 kWh (-0.87%) and 127,156 kWh (-1.40%), respectively.

The broad region of optimality around 28-32° suggests insensitivity to installation accuracy, which is a desirable characteristic in installation tolerance. A related graphic in the corner of the figure indicates that 30° is a fair compromise between winter (marginally non-optimal) and summer (near-optimal) performance conditions. The parametric study results are given in Figure 3, verifying 30° as an optimal trade-off between performance and system complexity.

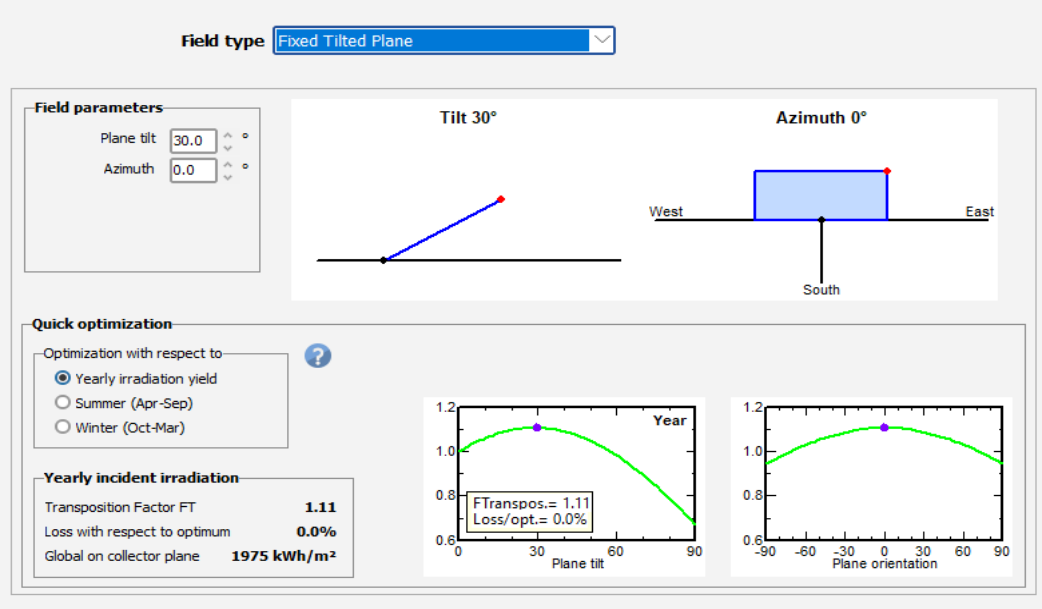

Figure 3. confirming that 30°

2.7 PVsyst Simulation Procedure

Full performance simulation was carried out using PVsyst 7.2 software [18], as follows in a systematic procedure:

1) Project Definition and Meteorological Data

It was defined as a grid-connected system with no battery storage at a particular geographical coordinate. Weather data was imported from a merged Meteonorm 8.0 database, including hourly data for Global Horizontal Irradiation (GHI), Diffuse Horizontal Irradiation (DHI), Ambient Temperature, and Wind speed. Validation of data was done through comparison with actual NASA POWER measurements, with an average error of 3% in annual GHI and a value of 1.2°C for average Temperature.

2) System Sizing and Configuration

Array configuration data was entered by selecting module types, number of modules, and electric string configuration. Inverter data was entered, such as efficiency curve data, MPPT voltage ranges, and max input current values. Electrical compatibility was also checked to ensure that string voltages are within inverter specs across all temperatures (-10°C to 70°C).

3) Orientation and Mounting Parameters

Orientation is defined as 0° azimuth (program convention for true south) and a tilt angle of 30°. Mount type is entered as "free-standing structure" in order to use the correct thermal models. This program computes the tilted surface's effective irradiation components based on an isotropic sky distribution and user-supplied albedo values. The simulation of the system's performance was carried out by PVsyst.

The array is oriented at 0° azimuth, which is equivalent to the direction of 'True South'. The tilt value of 30° was adopted following parametric studies in PVsyst, as this value allows the harvesting of 98.2% of the theoretical maximum annual energy, thereby accounting for both seasonal and self-cleaning abilities against dust. The total irradiance on the array plane G_β is the sum of beam, diffuse, and ground-reflected components:

$$G_\beta = G_{b,\beta} + G_{d,\beta} + G_{r,\beta} \quad (1)$$

Here $G_\beta = G_{b,\beta} + G_{d,\beta} + G_{r,\beta}$ is the beam component (with beam normal irradiance and theta z = 90, alpha the zenith angle),

$$G_{d,\beta} = G_{dh}\frac{1+\cos\beta}{2} \quad (2)$$

Is the isotropic diffuse component G_{dh} is diffuse horizontal irradiance, and

$$G_{r,\beta} = G_h\,\rho\,\frac{1-\cos\beta}{2} \quad (3)$$

Is the ground-reflected component ($G_{r,\beta}$ Global horizontal irradiance, ground albedo). The incidence-angle modifier IAM accounts for angular losses. Finally, the effective irradiance on the modules is:

$$G_{eff} = G_\beta \times IAM(\theta) \times (1 - L_{soil}) \quad (4)$$

Where L_{soil} (0.02) represents soiling loss. (For the Tajoura site, G_{eff} Approx 1886 mathrm kWh/m^2/yr as noted in the analysis.

4) Thermal Modeling

The working temperature of the module, an essential parameter for optimal functioning, was studied in the PVsyst software by assigning a value of 27 W/m²K as the "free-standing" and well-ventilated mounting system of the carport, thereby benefiting from the cooling effect of the coastal winds.

The electrical output begins with the module operating temperature. The cell temperature $\boldsymbol{T_{cell}}$ Can be modeled by:

Where $\boldsymbol{T_{amb}}$ is ambient temperature, =1000 W/m2, $\boldsymbol{k_T}$, is a wind cooling coefficient, the wind speed. For well-ventilated carport arrays, a simplified form is often used:

$$T_{cell} = T_{amb} + \frac{G_{eff}}{800}\,k_T \quad (5)$$

The module DC power then follows the irradiance and temperature dependence, where P_{module} =525W (module rated power) and gamma P=-0.0034C is the power temperature coefficient. For an array of $N_{modules}$ =150 modules, the maximum-power-point DC array output is:

$$P_{array,MPP} = N_{modules}\,P_{module}\,(1 + \Delta\eta_{qual})\,(1 - L_{LID})\,(1 - L_{mismatch}) \quad (6)$$

Accounting for a quality tolerance. The DC output after wiring losses is

$$P_{DC,out} = P_{array,MPP} \times (1 - L_{cable,DC}) \quad (7)$$

Where the DC cable loss $L_{cable,DC}$ (about 0.9%) depends on line length, current, and resistance. Finally, the AC power delivered to the grid is

$$P_{AC} = P_{DC,out}\,\eta_{inv}\,(1 - L_{night})\,(1 - L_{unavail}) \quad (8)$$

Using inverter efficiency η_{inv} Approx. 0.9762 and accounting for small parasitic (night) and availability losses.

5) Loss Parameters

The net AC energy can also be expressed by cascading all efficiency factors. For example, one formulation writes.

$$E_{AC} = E_h \times F_{tilt} \times F_{IAM} \times F_{soil} \times \eta_{PV} \times F_{temp} \times F_{qual} \times F_{LID} \times F_{mismatch} \times F_{cable,DC} \times \eta_{inv} \times F_{night} \times F_{unavail} \quad (9)$$

Where each F is a fractional loss/gain factor. For the Tajoura system, the factors were estimated as: F_{tilt}=1.099 (9.9% gain from the optimized 30° tilt), F_{IAM}=0.980, F_{soil}=0.980, F_{temp}=0.9796 (–2.04% from operating temperature), F_{qual}=1.0075, F_{LID}=0.980, $F_{mismatch}$=0.995, and $F_{cable,DC}$=0.991. The product of these and the inverter/night/unavailability efficiencies gives a total system efficiency η_{inv} approx 0.1768 (17.68%), consistent with the PVsyst simulation results.

Detailed loss components are set as described in Table 1. This specifically covers preconversion losses (soiling, angle of incidence), conversion losses (quality of modules, temperature effect, mismatch loss), DC system loss (cables' resistance), AC conversion loss (conversion efficiency inverter), and loss of availability (maintenance, failures). Values were selected based on manufacturer specifications, regional experience, and conservative engineering assumptions [19,20].

Table 1. PVsyst Loss Parameters

Loss Category	**Parameter**	**Value**
Pre-Conversion	Soiling (dust, dirt)	2.0%
	Incidence angle modifier	Manufacturer data
	Albedo (asphalt surface)	0.20
Conversion	Module quality variation	-0.75%
	Light-induced degradation	-2.0%
	Module temperature	Variable (-0.34%/°C)
	Mismatch and MPPT	Program calculated
DC System	DC cable resistive losses	0.90%
AC Conversion	Inverter efficiency	Manufacturer curve
	Inverter night consumption	0.04%
Availability	System unavailability	0.5% annually

5) 3D Scene Integration

The SketchUp structural model was imported to PVsyst to enable near-shading analysis and horizon profile verification. PVsyst 3D shading analysis visualization showing the imported SketchUp model with sun-path trajectories overlaid for the full annual cycle. The analysis confirms zero near-field shading from structural components throughout operational hours (6:00-18:00) across all seasons. Horizon profile (shown in blue line at bottom) indicates unobstructed southern exposure with elevation angles below 2° from 90° east to 270° west.

Color gradation represents solar altitude angles, with red indicating summer solstice paths, yellow indicating equinoxes, and blue indicating winter solstice. The open site configuration eliminates shading losses, validated through hourly simulation of 8,760 annual hours. As shown in the figure. 4, the open site configuration produces zero shading losses throughout the year, validated through hourly sun-path simulation.

Figure 4. the zero shading losses throughout the year

6) Simulation Execution

An annual simulation was executed with hourly time-step resolution. The program calculates hour-by-hour irradiation, module temperature, DC power output, inverter conversion, and AC energy production. Monte Carlo analysis with 100 iterations measures the uncertainty of product output estimates, and P50, P90, and P95 values are calculated for financial risk analysis.

2.8 Energy Modeling of PV Solar System

The energy produced by a PV solar module is estimated as:

$$E_{PV} = P_{STC}\left[1 + \beta_p(T_{cell} - T_{STC})\right]\frac{H_t}{H_{STC}} \quad (10)$$

Where: T_{STC} and T_{cell} are the cell's surface temperature at Standard Test Conditions and under real operation conditions (°C), $\beta_p$is the power temperature coefficient (%/°C), and H_{STC} and H_t Are the STC and real global solar irradiance incidents on the PV module surface. The challenge that researchers will face is to find an empirical equation to determine the cell surface temperature. T_{cell} For example:

$$T_{cell} = T_\infty + 7.8 \times 10^{-2} H_t \quad (11)$$

2.9 Economic Analysis Framework

Financial analysis utilized common criteria for evaluating renewable energy projects [26]. The cost of installation was calculated between 1,000 and 1,100 per kW of installed capacity based upon prevailing market rates for similar systems, such as modules, inverters, installation structure, electric materials, and installation costs. Operating and maintenance costs of 1.5 percent per year of installation costs were considered, similar to a grid-connected non-single-axis tracking and non-storing PV system. The leveled cost of energy (LCOE) is calculated as follows:

The Levelized Cost of Energy (LCOE) and the payback time money (PBTM). The cost of environmental damage produced by carbon dioxide (C_{CO2}) may be used to compute LCOE using the following equation:

$$LCOE = \frac{\left(\frac{r(1+r)^n}{(1+r)^n - 1}\right) \times C + C_{O\&M} - C_{CO2}}{E_t} \quad (12)$$

Where: r represents the real discount rate (2.4%), n denotes the plant lifespan, which is 25 years: C and $C_{O\&M}$ denote the capital cost, and operation in $, and maintenance expenditures $/year, respectively, C_{CO2} is the annual CO2 social cost $/yeat, and E_t represents the annual electricity provided by the PV system, kWh/year.

$$PBTM = \frac{C}{I_{ele} + I_{CO2}} \quad (13)$$

Where I_{Ele} and I_{Env} are the annual income from electricity selling and from CO_2 emission prevention ($/year). The cost of environmental damage (C_{CO2}) caused by CO_2 gas can be calculated by the following equation [29].

$$C_{CO2} = EF_{CO2} \times E_t \times \emptyset_{CO2} \quad (14)$$

Where: EF_{CO2} represents the CO_2 emission factor of the electric power generation system (kg CO_2/kWh), $\emptyset_{CO2}$ represents the carbon social cost ($/ton CO_2), which may be considered as $ 70/ton CO_2.

Where *It* stands for the costs of capital and operation & maintenance in year *t, Σt* is the electricity produced in year t, considering a 0.5% annual degradation rate, *r* is the real interest rate at 2.4%, and the sum is considered for a 25-year lifespan of the system. Net present value and internal rate of return were calculated using the formulas, considering a value of electricity of $0.10 per kWh based on commercial Libyan rates.

2.10 Assumptions, Limitations, Validation, and Uncertainty Quantification

The current study employs the following assumptions to streamline the analysis:

- Neglecting loss due to connections between devices;
- Constant efficiency of equipment;
- Discounting the salvage cost of the equipment at the end of the economic assessment.
- No shadowing occurred on the PV modules.
- Neglecting the time- performance degradation of the devices;

One of the main limitations of this work is the lack of sensitivity analysis for the key parameters affecting the decision-making process, such as the capital, operation, and maintenance expenditures, the real interest rate, and the CO2 price. Simulation results were validated in several ways [33]:

1. Cross-Tool Validation: Comparison of PVsyst's annual irradiation predictions with Global Solar Atlas values showed a deviation of less than 2%.

2. Meteorological Validation - Temperatures calculated by PVsyst's thermal analysis program were validated against NASA POWER temperatures with a 3°C agreement in module temperatures.

3. Electrical Validation: String layouts have been validated against inverter data through independent calculations.

The uncertainty in this research arises primarily from the data, model selection, and parameter estimation. For instance, the productivity of solar energy is highly dependent on climatic conditions, which can significantly influence the power generation profiles of the associated system. Additionally, the costs of renewable energy projects introduce further uncertainty. As noted by [34, 35], PV panel prices can vary by over 360%, ranging from $980 to $4,510 per kW.

3. Results

3.1 System Performance Overview

Mathematical simulations with PVsyst indicate an average annual power output of 128,964 kWh with a performance ratio of 83.37% and a specific yield of 1,637 kWh per kW per year. This performance is well above average for fixed systems at a similar latitude. The capacity factor of 18.69% represents a system's actual output compared to its theoretical max power output for a system of its type at a similar latitude that is fixed in place.

This is 48.70%. This is based on 24-hour system capacity and not just hours of power produced. In daylight hours of system operation, when power is produced, average load fulfillment is well above this average value. Total institutional load consumption over the simulation period is 10,609 kWh, 5,166.5 kWh of which is self-consumed, while 123,757 is fed to the grid. Another 5,442.5 kWh is drawn from the grid at night and during periods of low power production.

3.2 Solar Resource Utilization

Average yearly GHI at the location is 1,787 kWh/m², with a diffuse component of 799 kWh/m² (44.7% of total). This is a high value of the diffuse component, characteristic of a Mediterranean climate near a body of water. This makes a system's dependence upon accurate tracking less important while ensuring a high overall radiation value. Yield improvement through orientation and tilt optimization raises annual radiation collection by 9.9% compared to a flat mount. Global radiation on the surface of the collector is 1,964 kWh/m² yearly. After correcting for incidence angle modifier (IAM) and soiling, the overall radiation received by the PV energy conversion surface is 1,886 kWh/m² yearly. This is 96.0% collection of surplus radiation, with 4.0% loss, split 2.0% for IAM and 2.0% soiling.

An annual variation of 1.69 exists in monthly production from a peak summer value of 14,125 kWh in July to a low winter value of 8,347 kWh in December. This is a moderate value that prevents economic problems of either total system over-capacity or under-production in summer or winter months, respectively.

A monthly energy product and total solar radiation curve illustrating a relationship through annual data points between total solar radiation and overall system output. Major y-axis (blue bars, left) charts monthly AC system energy production in units of 1,000 kW/h from a low of 8,347 in December to a peak of 14,125 in July. Secondary y-axis (red line, right) charts global irradiation of the collecting surface in units of 1,000 kW/h from a low value of 130.4 in December to a peak value of 239.5 in July.

This close tracking of production and irradiation data strongly supports that system performance is limited by radiation. Some differences in tracking in summer (May through August) indicate differences in winter efficiencies of 1.2 percent to 1.5 percent compared to 2.8 percent to 3.2 percent for summer. A system with a 1.69:1 seasonal output profile (summer peak to winter valley) suggests a steady power output suitable for load servicing. Figure 5 - Clearance match of system output with monthly differences of isolation and a moderate factor from temperatures.

Figure 5. production closely

3.3 Comprehensive Loss Analysis

The PVsyst loss diagram quantifies energy flow from incident solar radiation through all loss mechanisms to final grid injection, as detailed in Table 2. Starting from 1,787 kWh/m² annual GHI, successive loss stages include:

Table 2. Comprehensive System Loss Breakdown

Stage	Energy Flow	Loss Type	Loss (%)	Cumulative Loss (%)
GHI	1,787 kWh/m²	-	-	-
Tilt optimization	1,964 kWh/m²	Gain	+9.9	+9.9

IAM losses	1,925 kWh/m²	Optical	-2.0	+7.7
Soiling	1,886 kWh/m²	Environmental	-2.0	+5.5
PV conversion (STC)	148,535 kWh	-	-	-
Irradiance level	147,808 kWh	Low-light	-0.49	-
Module quality	148,916 kWh	Manufacturing	+0.75	-
LID	145,939 kWh	Degradation	-2.0	-
Temperature	142,964 kWh	Thermal	-2.04	-
Array at MPP	143,926 kWh	-	-	-3.1
DC cables	132,656 kWh	Resistive	-0.90	-3.9
Inverter	129,451 kWh	Conversion	-2.38	-6.2
Night	129,400 kWh	Parasitic	-0.04	-6.2
Unavailability	128,964 kWh	Maintenance	-0.41	-6.6
Final AC output	**128,964 kWh**	**Total**	**-13.2**	**-13.2**

Comprehensive system loss diagram from PVsyst showing energy transformation from incident solar radiation to grid-injected AC power. The Sankey-style diagram illustrates energy flow through successive stages:

(1) Global horizontal irradiation (1,787 kWh/m²/year) modified by tilt optimization (+9.9% gain to 1,964 kWh/m²),
(2) Pre-conversion losses from IAM effects (-2.0%) and soiling (-2.0%), reducing effective irradiation to 1,886 kWh/m²,
(3) PV conversion at STC efficiency (20.36%), yielding nominal 148,535 kWh with adjustments for irradiance level (-0.49%), module quality (+0.75%), LID (-2.0%), and temperature effects (-2.04%), producing 143,926 kWh at array MPP,
(4) DC system losses from cable resistance (-0.90%), reducing output to 132,656 kWh,
(5) AC conversion through inverters (-2.38%) and night consumption (-0.04%) yielding 129,400 kWh,
(6) System unavailability (-0.41%) resulting in final grid injection of 128,964 kWh. Color coding indicates loss categories: red for thermal/environmental, orange for electrical, blue for conversion efficiency, and green for availability. Total system losses from array MPP to grid injection amount to 13.2%, dominated by inverter conversion, thermal effects, LID, and soiling.

Total losses from array maximum power point to grid injection amount to 13.2%, dominated by inverter conversion (2.38%), module temperature effects (2.04%), light-induced degradation (2.0%), and soiling (2.0%). This loss profile aligns with expectations for grid-connected systems in warm climates with moderate dust exposure. The complete energy flow pathway is illustrated in the figure. 6.

3.4 Thermal Performance Analysis

Module operating temperature significantly impacts conversion efficiency through the negative temperature coefficient (-0.34%/°C for the selected modules). Monthly average module temperatures range from 18-22°C in winter (December-February) to 42-48°C in summer (June-August). Temperature differences between modules and the environment (expressed as a shaded area) of 8-12°C represent a balance of heating from incident irradiation and cooling from coastal winds. Dashed lines represent STC Reference Temperature (25°C) and Critical Temperature Threshold (70°C).

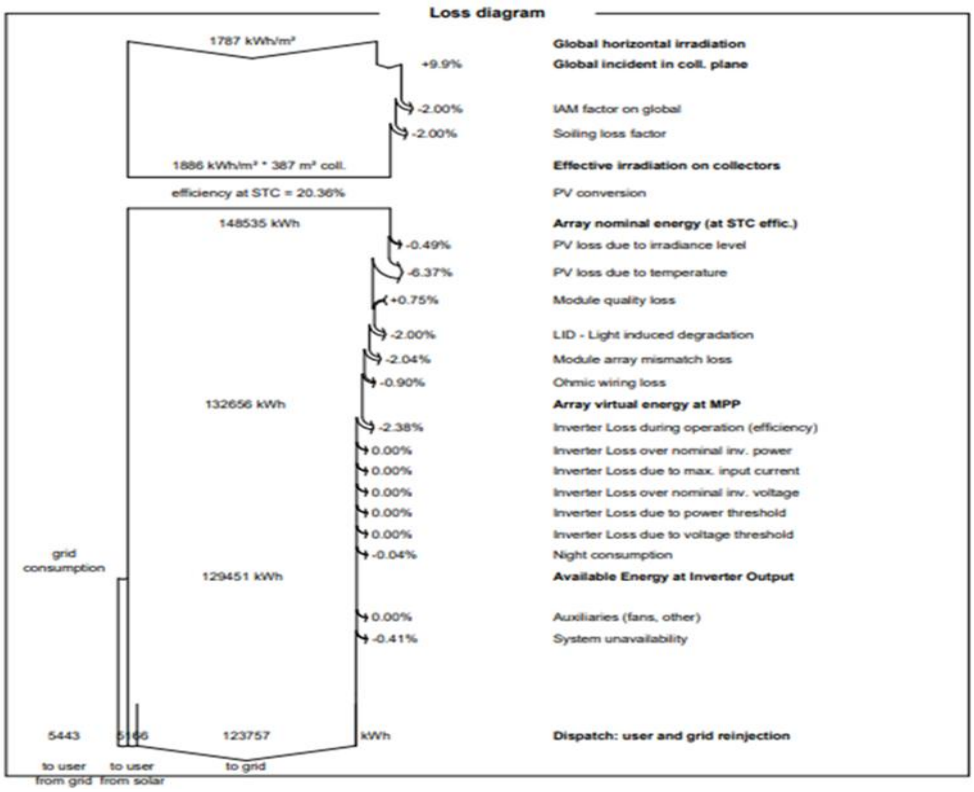

Figure 6. The complete energy flow pathway

Graphic overlays express the rate of power loss per STC units of temperature per month as a value of -1.2% to -3.2%. Free-standing mount with back vent cooling, together with 7 m/s average wind speeds in coastal areas, leads to a decrease in cell temperatures of 5-7°C compared to roof-mounted designs, attributable to a 1.5-2.0% improvement in annual efficiencies. This demonstrates the advantage of the site's Mediterranean coastal location for PV applications. Detailed thermal performance data are presented in the Figure. 7.

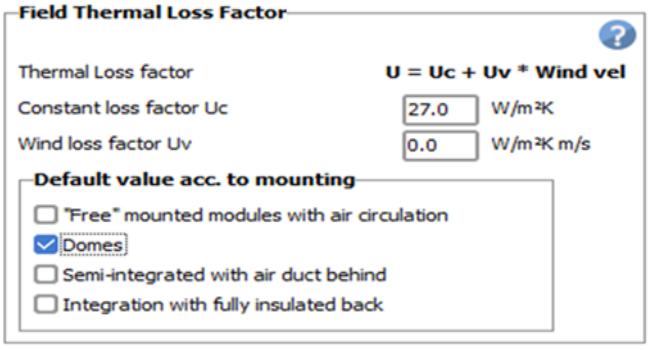

Figure 7. Detailed thermal performance data

3.5 Subsystem Performance

The performance metrics of individual subsystems are shown in Table 3. Both subsystems have identical performance ratios of 83.28 percent in college mode and 83.41 percent in hospital mode, thus verifying a balanced design and an optimized electrical configuration. This 0.13 percentage point difference is within simulation error margins and is likely because of inverter performance differences at lower loads.

Table 3. Subsystem performance metrics

Parameter	College System	Hospital System	Combined
Array capacity	19.95 kWp	58.80 kWp	78.75 kWp
Module count	38	112	150
Inverter capacity	20 kW	100 kW (2×50)	120 kW
Annual production	33,147 kWh	95,817 kWh	128,964 kWh
Specific yield	1,657 kWh/kWp	1,652 kWh/kWp	1,637 kWh/kWp
Performance ratio	83.28%	83.41%	83.37%
Capacity factor	18.98%	18.61%	18.69%

In fact, redundancy is also achieved within the hospital subsystem through a dual-inverter configuration that allows maximum MPPT tracking of the overall array. This is achieved because all individual hospital inverters run at an average of 29 kW (equivalent to 58% of their capacity) in order to maximize efficiencies.

3.6 Monthly and Annual Production Profile

The monthly details are encapsulated in Table 4, illustrating output, consumption, self-cons, and grid interactions. Peak output is recorded in summer periods (May to August) at an average of 13,560 kWh/month. The average output in winter periods (November to February) is 9,176 kWh/month. This 47.7% seasonal variation is quite low compared to areas that are geographically located at higher latitudes.

Only 4.0% of total production is consumed directly. 96.0% of production is sent to the grid. This is due to the configuration of the system, which is grid-connected, and the system does not have any storage. This is also due to the peak production hours not aligning with the institutionally distributed load, which occurs mid-day. Potential revenue from net metering is represented by the 118,315 kWh of net export to the grid, which is the export minus import of the grid annually.

There is a monthly grid interaction analysis that shows the production, export, import, and net energy flow analysis throughout the year. The stacked bar graph shows monthly production, which is represented by the blue bars (left y-axis, in kWh), ranging from 8,347 kWh in December to 14,125 kWh in July. The direct self-consumption, which is the green portion of the bars, is relatively constant at 338-556 kWh/month, which is 4.0% of total annual production. Export to the grid, which is the orange portion, follows production closely at 8,009-13,569 kWh/month.

The grid import, which is represented by the red line on the right y-axis, corresponds to nighttime and low-production period demands and remains stable at 388-501 kWh/month. The black line indicates net grid export ("export minus import") of 118,315 kWh annually. The high export percentage, at 96.0% is due to institutional operations, which are concentrated. This is also due to the system being grid-connected and not having storage, as well as peak demand timings misalignment, which occurs mid-day. As shown in the figure. 8, monthly export patterns closely follow production, with import requirements remaining relatively constant throughout the year at 400-500 kWh/month, corresponding to nighttime and low-production period demands.

3.7 Probabilistic Production Forecasting

Monte Carlo uncertainty analysis quantifies production variability from meteorological fluctuations, system performance variations, and modeling uncertainties. Results are presented in Table V using standard probability levels for renewable energy project financing.

Table 4. Monthly energy flows (kwh)

Month	GHI (kWh/m²)	Collector Irrad.	Ambient Temp. (°C)	Production	Self-Cons.	Export	Import
Jan	102.4	138.2	13.8	9,245	387	8,858	412
Feb	115.3	145.6	14.2	9,876	398	9,478	438
Mar	162.8	188.4	16.5	12,134	456	11,678	489
Apr	185.2	197.3	19.8	12,456	478	11,978	456
May	218.6	222.1	23.6	13,678	512	13,166	478
Jun	236.4	232.8	26.9	13,892	534	13,358	445
Jul	245.8	239.5	28.4	14,125	556	13,569	434
Aug	228.7	228.2	28.8	13,534	528	13,006	445
Sep	189.3	199.8	26.2	11,987	467	11,520	467
Oct	147.5	171.3	23.1	10,456	423	10,033	489
Nov	108.9	142.7	18.7	9,234	389	8,845	501
Dec	95.7	130.4	14.9	8,347	338	8,009	388
Annual	**1,786.6**	**1,963.7**	**21.2**	**128,964**	**5,167**	**123,757**	**5,443**

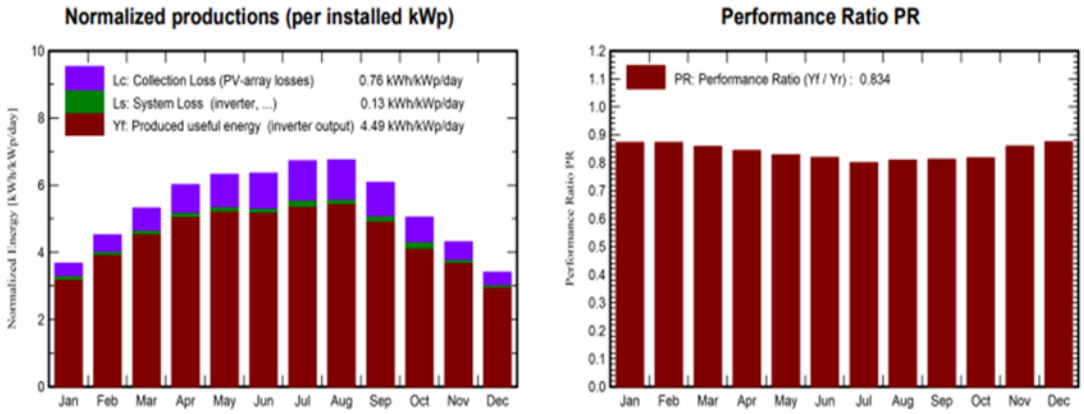

Figure 8. Monthly export patterns

Probability distribution of annual energy production showing cumulative distribution function (CDF) from Monte Carlo analysis with 100 iterations. “S-curve”: This is a representation of exceedance probability, with “horizontal axis” denoting annual “production (MWh)” ranging from 115 to 135, while “vertical axis” denotes “probability (%)” ranging from 0 to 100. Key probability levels are marked: P99 = 119.67 MWh (99% confidence), P95 = 121.89 MWh (95% confidence), P90 = 123.28 MWh (90% confidence, typically used for debt service calculations), P75 = 126.10 MWh (75% confidence), and P50 = 128.92 MWh (median, best estimate for equity returns). Shaded areas represent ranges of uncertainty, P50-P90 spread of 5.64 MWh (4.4 %) in light blue, and P50-P95 spread of 7.03 MWh (5.5 %) in dark blue.

Table 5. Probabilistic production forecast

Probability Level	Definition	Annual Production (MWh)	Deviation from P50
P50	50% exceedance	128.92	Baseline
P75	75% exceedance	126.10	-2.2%
P90	90% exceedance	123.28	-4.4%
P95	95% exceedance	121.89	-5.5%
P99	99% exceedance	119.67	-7.2%

This suggests a robust expectation of production in stable conditions in Tajoura's steady solar resource. This is supported by a narrow PDF overlap, or a normal distribution in a standard deviation of 2.8 MWh around P50. This allows for meteorological variability of ± 8% annual GHI, component degradation of ± 0.2% annual rate, as well as performance assumptions of ± 3% PR. Note that a small spread of probabilities (P50-P90 of 5.64 MWh or 4.4%) suggests a robust expectation of production in stable conditions in Tajoura's steady solar resource. In finance, P90 is commonly used for debt service in a proposed project, as a means of projecting a cautious expectation of production at 90% confidence. P50 is also a robust means of projecting a best estimate of returns for equity investment. This full distribution is represented in Figure 9.

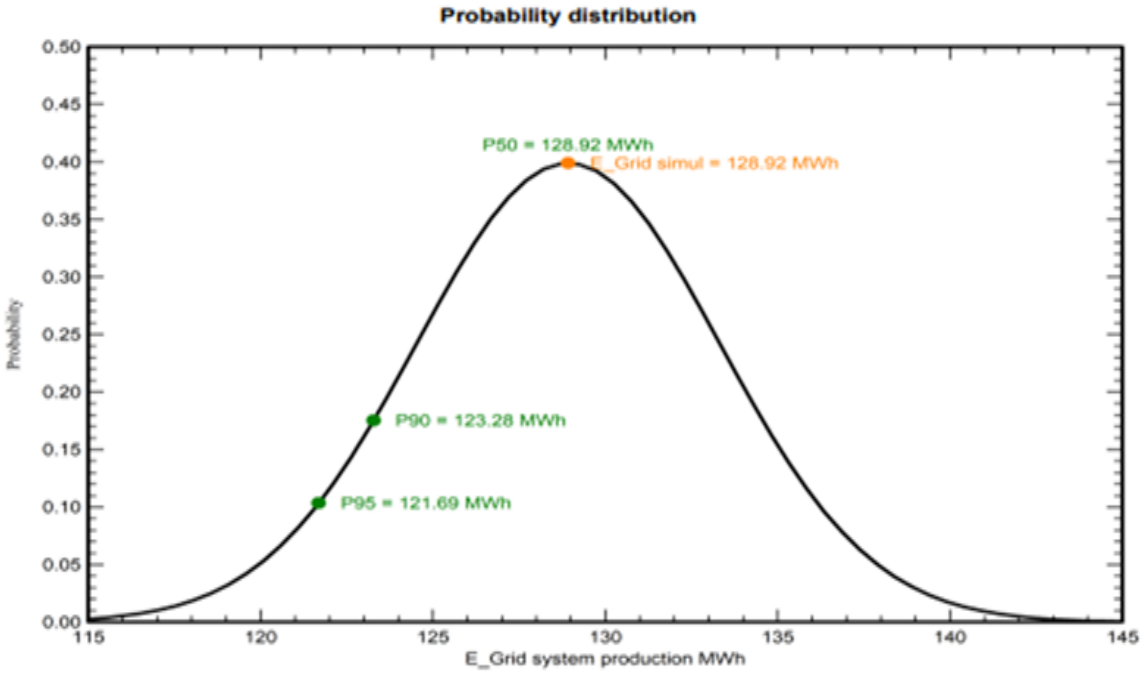

Figure 9. The complete probability distribution

3.4 Economic Performance Metrics

Detailed results of financial analysis are presented in Table 6, considering a capital investment of $78,000 and a value of energy of $0.10 per kW. Sensitivity analysis based on important variables will be discussed in later sections.

An LCOE of $0.052-$0.057 per kilowatt hour is attractive compared to grid electricity in Libya, priced at $0.08-$0.12 per kilowatt hour, thus offering a 33%-46% cheaper alternative. Payback periods of 6.1-6.7 years offer excellent returns with well over 18 years of positive cash flows within a 25-year warranty period for the modules. An IRR of 14.8%-16.3% is much higher than alternative investment returns,

ensuring that overall project economics are excellent. Other economic benefits include grid sales of electricity. At wholesale costs of $0.05-$0.08 per kilowatt hour, the annual surplus of 123,757 kilowatt hours translates to an extra 6,188-$9,900 per annum of electricity that could be sold back to the grid.

Table 6. Economic performance metrics

Metric	Value	Units
Capital cost	$78,000	USD
Annual O&M cost	$3,170	USD/year
Year 1 production	128,964	KWh
Year 1 revenue	$12,896	USD
25-year production	3,224,100	KWh
LCOE (real, 6% discount)	$0.052-0.057	USD/kWh
Simple payback period	6.1-6.7	Years
Discounted payback	8.2-9.1	Years
NPV (25-year, 6% discount)	$83,890	USD
IRR	14.8-16.3	%
Benefit-cost ratio	1.82	-

3.5 Environmental Impact Assessment

Emissions per year are reduced by 70.93 metric tons of CO_2, calculated based on a grid emissions factor of 1.073 kg of CO_2 per kWh. On an average system lifetime of 25 years, total emissions avoided amount to 3,460 metric tons of CO_2. This is comparable to taking 773 vehicles off-road for a year or the annual carbon sequestration service of 4,025 acres of forests. Factors in a lifecycle assessment include embodied carbon emissions from manufacturing, transportation, and installation of 1,560 metric tons of CO2 equivalents. Energy payback time is 2.1 to 2.4 years, while carbon payback time is 22 months. Net carbon savings of 1,617 metric tons in a lifetime offer 91% benefits after factoring in embodied impacts.

Other environmental advantages include an average annual conserved volume of 193,000 to 322,000 liters of WATER compared to thermoelectric power plants, which consume 1.5 to 2.5 liters per kilowatt-hour in fossil fuel plants, especially in arid Libya. This also entails a decrease of 128 kg/yr of sulfur dioxide emissions, 94 kg/yr of nitrogen oxides, as well as 6.2 kg/yr of particulate matter. The current state of the environmental effects of PV power plants amidst these evolving conditions regarding CO2 emissions, land use, pollutant and noise emissions, and water usage, and to develop an environmental management plan to reduce the adverse impact of PV has been presented.

3.6 Grid Interaction Analysis

This large export share, 96.0 per cent of total production, can be attributed to a combination of several interrelated factors, such as the prevalence of daytime institutional operations, a grid-connected structure, which is without energy stored, and load-profile peculiarities. Monthly export volumes show a close relationship with the production rates, whereas import demands also do not vary much throughout the calendar year, with an average of 400-500kWh per month, hence indicating the needs during the night and low-production periods. The annual net grid export is 118,315 kWh, which is a larger surplus that could be realised by feed-in tariffs or net-metering schemes. This redundancy both provides the ability to support future scale increases of load without the need to augment the system and can also support increased scale increases to photovoltaic generation beyond those of an institution, thereby supporting the goal of broader grid decarbonisation. The grid-interactive nature of the installation requires very close collaboration with utility operators. In addition, the standards used in exported power should comply with the grid code requirements of voltage frequency and harmonic distortions. Huawei inverters selected have anti-islanding protection, reactive-power control, and fault-ride-through capabilities, and as such, they meet the established international standards, that is, the IEEE 1547 and IEC 61727.

4. Conclusions

Developed and modeled a 78 kW grid-connected PV carport system for College of Renewable Energy—Tajoura attains satisfactory technical performance metrics of PR = 83.37%, specific energy output Yf = 1,637 kWh/kWp/yr, and a SF of ca. 48.7%, thereby offering substantial daytime load shifting capabilities. Aggregate yearly electricity output is approximately 129 MWh (post-loss analysis), and loss component validation leads to a clear identification of dominant soiling, thermal, LID, electrical connection, and inversion loss components. On the economic front, it attains an attractive Levelized Cost of Electricity (LCOE) of $0.052–0.057 per kWh, a Simple Payback Period of 6–7 years, and attractive investment returns with an NPV of approx. 16,890–83,890 and an IRR of 14.8–16.3%. From an environmental perspective, it prevents emissions of 71tCO_2/yr, with total lifetime emissions avoided of 1,600+CO_2 after accounting for embodied emissions. The integrated SketchUp–PVsyst workflow provides validated, site-specific results and a replicable design template for similar institutional deployments in North Africa.

5. Acknowledgment

The authors would like to extend their appreciation to the College of Renewable Energy administration at Tajoura and Tajoura Kidney Hospital for allowing them to make use of the facilities and data. Gratitude is also expressed for assistance received from technical staff.

REFERENCES

[1] Y. Nassar, M. Irhouma and M. Salem, "Towards Green Economy: Case of Electricity Generation Sector in Libya," *Solar Energy and Sustainable Development Journal,* vol. 14, no. 1, p. 334–360, 2025. https://doi.org/10.51646/jsesd.v14i1.549

[2] H. El-Khozondar, et al. "Technical and Environmental Cost-Benefit Analysis of Strategies towards a Green Economy in the Electricity Sector in Libya," *Economics and Policy of Energy and the Environment*, 2025. Under publication.

[3] Libyan Authority for Electricity and Renewable Energy, *Annual Statistical Report*. Tripoli, Libya: Libyan Authority for Electricity and Renewable Energy, 2023.

[4] Y. Siregar, Y. Hutahuruk, and Suherman, "Optimization design and simulating solar PV system using PVSyst software," in *Proc. 4th Int. Conf. Electrical, Telecommun. Comput. Eng. (ELTICOM)*, Medan, Indonesia, Sep. 2020, pp. 219–223, doi: 10.1109/ELTICOM50775.2020.9230474.

[5] H. Awad, et al., "Optimal design and economic feasibility of rooftop photovoltaic energy system for Assuit University, Egypt," *Ain Shams Engineering Journal*, vol. 13, no. 3, p. 101599, 2022. https://doi.org/10.1016/j.asej.2021.09.026.

[6] A. Chiasson, "Solar carport systems: Economic and energy analysis of hospital parking applications," *Sol. Energy*, vol. 160, pp. 154–163, Jan. 2018, doi: 10.1016/j.solener.2017.11.070.

[7] S. Mohammed, M. El-Sheikh, and M. Abdelrahman, "PV system performance in car parking applications: A case study using PVSyst," *J. Renew. Energy Eng.*, vol. 45, no. 2, pp. 110–121, 2020.

[8] International Renewable Energy Agency, *Renewable Energy Prospects for North Africa*. Abu Dhabi, UAE: IRENA, 2019.

[9] NASA POWER Project, "Prediction of Worldwide Energy Resources," NASA Langley Research Center. [Online]. Available: https://power.larc.nasa.gov. Accessed: Jan. 15, 2025.

[10] A. Elmabruk, M. Salem, M. Khaleel, and A. Mansour, "Prediction of Wind Energy Potential in Tajoura and Mislata Cities," *Wadi Alshatti University Journal of Pure and Applied Sciences*, vol. 3, no. 2, pp. 125-131, 2025. https://doi.org/10.63318/waujpasv3i2_17

[11] M. Khaleel, et al., "Solar and wind atlas for Libya," International Journal of Electrical Engineering and Sustainability (IJEES), vol. 1, no. 3, pp. 27-43, 2023. https://ijees.org/index.php/ijees/article/view/44

[12] B. Ahmed, et al. "Atlas of solar (PV and CSP) and wind energy technologies in Libya ".The North African Journal of Scientific Publishing (NAJSP), vol. 1, no. 4, pp. 8-24, 2023. https://www.researchgate.net/publication/374846048

[13] G. Miskeen, et al., "Mapping of PV solar module technologies across Libyan Territory," in Iraqi International Conference on Communication and Information Technologies (IICCIT), Basrah, Iraq, 07-08 September

2022. https://doi.org/ 10.1109/IICCIT55816.2022.10010476

[14] R. Kumar, C. S. Rajoria, A. Sharma, and S. Suhag, "Design and simulation of standalone solar PV system using PVsyst software: A case study," Mater. Today Proc., vol. 46, no. 11, pp. 5322–5328, 2021, doi: 10.1016/j.matpr.2020.08.785.

[15] Y. Fathi, et al. "Atlas of PV Solar Systems Across Libyan Territory," 2022 International Conference on Engineering & MIS (ICEMIS), Istanbul, Turkey, 2022, pp. 1-6, doi: 10.1109/ICEMIS56295.2022.9914355.

[16] B. K. Nallamothu, R. Janga, and S. R. Pendem, "Design and analysis of grid connected solar PV system using PVsyst software," in Proc. IEEE Students Conf. Eng. Syst. (SCES), Prayagraj, India, Jun. 2024, pp. 1–6, doi: 10.1109/SCES61914.2024.10652298.

[17] S. Alsadi, and K. Amer, "General polynomial for optimizing the tilt angle of flat solar energy harvesters based on ASHRAE clear sky model in mid and high latitudes," Energy and Power, vol. 6, no, 2, pp. 29-38, 2016 .https://doi.org/10.5923/j.ep.20160602.01

[18] A. Mermoud and B. Wittmer, "PVsyst 7 software," in Proc. 37th Eur. Photovolt. Solar Energy Conf. Exhib., Lisbon, Portugal, Sep. 2020, pp. 1473–1477.

[19] A. Alsharif, et al., "Mitigation of Dust Impact on Solar Photovoltaics Performance Considering Libyan Climate Zone: A Review," Wadi AlShatti University Journal of Pure and Applied Sciences, vol. 1, no. 1, pp. 22-27 .

[20] K. Amer, et al., "Power losses on PV solar fields: sensitivity analysis and a critical review," International Journal of Engineering Research & Technology (IJERT), vol. 9, no. 9, pp. 1000-1007, 2020. https://www.researchgate.net/publication/344520794